JOURNAL OF COMPUTATIONAL PHYSICS 74, 477–487 (1988)

The Free-Boundary Equilibrium Problem for Helically Symmetric Plasmas

H. J. GARDNER*, R. L. DEWAR, AND W. N-C. SY†

Department of Theoretical Physics, Research School of Physical Sciences, The Australian National University, Canberra A.C.T. 2601, Australia

Received December 19, 1986; revised May 13, 1987

An iterative technique for solving the ideal MHD equilibrium equations for a helically symmetric plasma with a free boundary is described. The method involves an application of Green's theorem and has been formulated for the geometry of a heliac. It is used to determine a stability diagram for the SHEILA heliac as a function of the plasma pressure and the current in one of the external coils. © 1988 Academic Press, Inc.

1. INTRODUCTION

Recently there has been considerable progress in the computation of three-dimensional magnetohydrodynamic equilibria with a free boundary [1, 2]. In spite of this, two-dimensional equilibrium and stability codes continue to be important approximate tools for the analysis of 3D (stellarator) plasma configurations [3]. In the limit of large aspect ratio, or large number of helical periods, stellators of the heliac type are particularly well approximated as being helically symmetric. Some of the recent interest in this sort of configuration has been inspired by the high $\langle\beta\rangle$ limits predicted by some helically symmetric fixed-boundary-equilibrium and stability studies [4–6].

In this paper we present an iterative method for solving the free-boundary helically symmetric, ideal equilibrium equations. The algorithm involves an application of Green's theorem to a model geometry which we take as being that of a generic heliac. The fixed-boundary flux coordinate version of the PEST equilibrium code, FEQ2.5 [7], has been modified to incorporate this algorithm. In Section 2 we describe the free-boundary equilibrium equations in some detail. The Green's function for the helical Grad–Shafranov equation is introduced in Section 3 and the new code, FEQ2.5 (FR), is described in Section 4. In Section 5 the code is used, along with other codes in the PEST series, to model the free-boundary equilibrium and stability of the SHEILA heliac [8].

* Present address: Max-Planck-Institut für Plasmaphysik, Boltzmannstr, D-8046 Garching b. München, F.R.G.

† Present address: School of Mathematical Sciences, New South Wales Institute of Technology, Broadway, NSW 2007, Australia.

0021-9991/88 $3.00

2. Green's Theorem for the Model Heliac

Consider the $l=1$, helically symmetric plasma and external coil configuration shown in Fig. 1. A straight conductor carrying a current I defines the z-axis of a cylindrical coordinate system (r, ϕ, z). It is completely enclosed by a solenoid, γ, which need not be circular in cross section, carrying a surface current $\mathbf{i}$. The plasma, region C, has a net longitudinal current, I_p, which we shall assume for the moment to be zero, and a surface current $\mathbf{i}_1$. There may also be some helical line currents in region B as will be discussed later.

All scalar equilibrium quantities are functions of r and $\zeta = \phi - hz$ only, where the constant h gives the helical pitch of the configuration. Any helically symmetric magnetic field can be written [7]

$$\mathbf{B} = h\mathbf{u} \times \nabla\psi + hg\mathbf{u}, \tag{1}$$

where $\mathbf{u} \equiv (\mathbf{e}_z + hr\mathbf{e}_\phi)/(1 + h^2r^2)$ and the stream function $\psi(r, \zeta)$ is such that the difference, $2\pi(\Delta\psi)$, between ψ on two helical lines (each of constant r and ζ) is equal to the flux through the helical ribbon which is defined by those lines and is of length $2\pi/h$ in the z direction. Similarly, $2\pi\,\Delta g/\mu_0$ is equal to the current through such a helical ribbon. Note that $g(r, \zeta)$, unlike $\psi(r, \zeta)$, does not contain an arbitrary constant. Its value at infinity is proportional to the total longitudinal current:

$$2\pi g_\infty = \mu_0 I_z. \tag{2}$$

(To show this, take the line integral of $\mathbf{B}$ along one twist of the symmetry vector, $\mathbf{u}$, at infinity and return along $\mathbf{e}_z$ and note that $\mathbf{B} \cdot \mathbf{e}_z = 0$ at infinity.)

The helically symmetric ideal equilibrium condition

$$\mathbf{J} \times \mathbf{B} = \nabla p \tag{3}$$

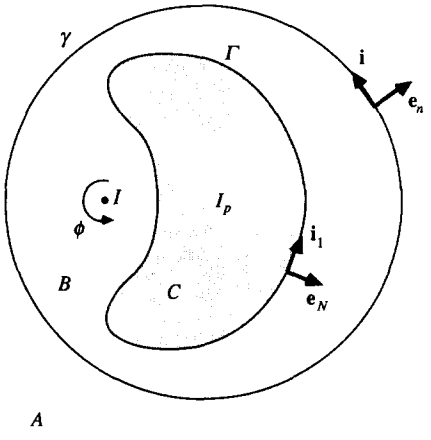

FIG. 1. Helically symmetric plasma and coil configuration as described in the text.

is equivalent to the helical Grad–Shafranov equation

$$\mathscr{L}(\psi) \equiv \nabla \cdot (\kappa \nabla \psi) = \frac{-2\kappa^2}{h}\, g(\psi) - \kappa g(\psi)\, g'(\psi) - \mu_0 p'(\psi), \tag{4}$$

where $\kappa \equiv h^2/(1+h^2r^2)$ is the sum of the squares of the curvature and torsion of a helical line of pitch h. Note that the transformation to $l>1$ equilibria, which are functions of r and $\zeta_l = l\phi - hz$ only, can be effected by changing the scale of h.

The equilibrium of Fig. 1 can be specified in terms of ψ by solving Eq. (4) inside the regions A, B, and C along with the boundary conditions across the plasma surface, Γ, and the solenoid, γ, and as $r \to 0$ and $r \to \infty$. The helical flux will diverge logarithmically at $r=0$ (due to the central conductor) and as $r \to \infty$ (due to the total longitudinal current). The jump conditions on the magnetic field across γ and Γ give rise to discontinuities in g and $\nabla\psi$. For the plasma surface these are

$$[\![g]\!]_\Gamma \equiv (g_B - g_C)|_\Gamma = \frac{\mu_0 \mathbf{i}_1 \cdot (\mathbf{e}_N \times \mathbf{u})}{h|\mathbf{u}|^2} \tag{5}$$

and

$$[\![\partial_N \psi]\!]_\Gamma = \frac{\mu_0 \mathbf{i}_1 \cdot \mathbf{u}}{h|\mathbf{u}|^2}, \tag{6}$$

where $\partial_N \psi \equiv \mathbf{e}_N \cdot \nabla\psi$ denotes the normal derivative of ψ on Γ. In equilibrium $\mathbf{i}_1$ must be compatible with the constraint of pressure balance and Γ must be a flux surface. The (constant) values of g in the vacuum regions may be found from Eq. (1). Within region C the g and p' profiles may be specified in accordance with some model of the plasma. If we let ψ be continuous across γ and Γ then there is one undetermined constant in the complete equation set [9].

Let G be a helically symmetric Green's function satisfying

$$\mathscr{L}[G(r, \zeta \mid r_0, \zeta_0)] = \frac{-4\pi}{r}\, \delta(r-r_0)\, \delta(\zeta - \zeta_0) \tag{7}$$

then Green's theorem, when applied to

$$G\mathscr{L}(\psi) - \psi\mathscr{L}(G) = \nabla \cdot (G\kappa\, \nabla\psi - \psi\kappa\, \nabla G)$$

integrated over one period of region C gives

$$\int_\Gamma \kappa(G\, \partial_N \psi_C - \psi_C\, \partial_N G)\, dS - \int G\mathscr{L}(\psi)\, dV = \begin{cases} 8\pi^2 h^{-1} \psi(r_0, \zeta_0) & (r_0, \zeta_0) \text{ in } C \\ 0 & (r_0, \zeta_0) \text{ outside } C. \end{cases} \tag{8}$$

The value of $\partial_N \psi_C$ on Γ can be expressed in terms of $\partial_N \psi_B$ using Eq. (6). Green's theorem can then be applied to regions B and A to give an integral expression for $\psi(r_0, \zeta_0)$ for (r_0, ζ_0) throughout $A \cup B \cup C$. The volume integral of $G\mathscr{L}(\psi)$ can be eliminated by introducing the auxiliary fields $\bar{\psi}$ and ψ_{vac}, where $\bar{\psi}$ is the solution to the fixed boundary problem (Eq. (4) with $\bar{\psi}|_\Gamma = 0$) in region C and ψ_{vac} is the vacuum flux of the external coils. Then $\mathscr{L}(\bar{\psi}) = \mathscr{L}(\psi)$ in region C and $\mathscr{L}(\psi_{\text{vac}}) = \mathscr{L}(\psi)$ in regions A and B and ψ_{vac} satisfies the same boundary conditions as ψ as $r \to 0$ and $r \to \infty$. Provided that the solution to the fixed-boundary problem is unique, we have

$$
\begin{aligned}
8\pi^2 h \;{}^1\psi(r_0, \zeta_0) = & \int_\Gamma \kappa [G\, \partial_N(\psi_{\text{vac}} - \bar{\psi}) - \psi_{\text{vac}}\, \partial_N G]\, dS \\
& + \begin{cases} 8\pi^2 h^{-1} \psi_{\text{vac}}(r_0, \zeta_0) & (r_0, \zeta_0) \text{ in } A \cup B \\ 8\pi^2 h^{-1} \bar{\psi}(r_0, \zeta_0) & (r_0, \zeta_0) \text{ in } C \\ 4\pi^2 h^{-1} \psi_{\text{vac}}(r_0, \zeta_0) & (r_0, \zeta_0) \text{ on } \Gamma \end{cases} \\
& - \int_\Gamma G\kappa \frac{\mu_0 \mathbf{i}_1 \cdot \mathbf{u}}{h|\mathbf{u}|^2}\, dS. \qquad (9)
\end{aligned}
$$

If there are extra helical currents in region B then their vacuum fluxes must be added to ψ_{vac} and the values of g adjusted accordingly. A net longitudinal plasma current, I_p, can be treated by adding to ψ_{vac} any flux function $\hat{\psi}$ which satisfies Ampère's law on paths enclosing region C. The simplest choices for $\hat{\psi}$ are $\hat{\psi}_1 = (\mu_0 I_p / 2\pi h) \ln r$ and $\hat{\psi}_2 = -(\mu_0 I_p / 2\pi h)(h^2 r^2 / 2)$, however, because $\psi_{\text{vac}} + \hat{\psi}$ will not satisfy the same boundary conditions as ψ, these will necessitate additional surface integrals at $r = 0$ and as $r \to \infty$ in Eq. (9). It turns out that these surface integrals can be eliminated by a judicious choice of the Green's functions G_1 and G_2 of the next section: if $\hat{\psi}_1$ is used then G_2 should be chosen and if $\hat{\psi}_2$ is used then G_1 should be chosen [9].

3. Choice of Green's Functions

Two solutions of the "fundamental" helical Grad–Shafranov equation, Eq. (7), are

$$
G_1(r, \zeta | r_0, \zeta_0) = \frac{-2}{h^2} \left(\ln r_> + \frac{1}{2} h^2 r_>^2 \right) + \bar{g} \qquad (10)
$$

and

$$
G_2(r, \zeta | r_0, \zeta_0) = \frac{2}{h^2} \left(\ln r_< + \frac{1}{2} h^2 r_<^2 \right) + \bar{g}, \qquad (11)
$$

where

$$\bar{g}(r, \zeta \mid r_0, \zeta_0) = -4rr_0 \sum_{n=1}^{\infty} I_n'(nhr_<)\, K_n'(nhr_>) \cos[n(\zeta - \zeta_0)] \tag{12}$$

and $r_> = \max(r, r_0)$, $r_< = \min(r, r_0)$.

This can be proved by expanding $\delta(\zeta - \zeta_0)$ and considering the coefficients of $\cos[n(\zeta - \zeta_0)]$ on either side of Eq. (8) [9, 10]. Each of these Green's functions corresponds to the helical flux due to a current loop. The current, of magnitude $(4\pi/\mu_0 h)$, flows in the $(-z)$ direction along the helix $(r = r_0, \zeta = \zeta_0)$, and returns along a path at infinity in the case of G_1, and along the z-axis in the case of G_2. Thus G_1 is equivalent to the integral expression

$$G_1(r, \zeta \mid r_0, \zeta_0) = -(r^2 + r_0^2) + \frac{1}{h^2} \int_{-\infty}^{\infty} \left\{ \frac{[1 + h^2 rr_0 \cos(\phi - \phi_0)]}{|\mathbf{r} - \mathbf{r}_0|} - \frac{1}{\sqrt{[(z - z_0)^2 + a^2]}} \right\} dz_0, \tag{13}$$

where $|\mathbf{r} - \mathbf{r}_0| = \{r^2 - 2rr_0 \cos(\phi - \phi_0) + (z - z_0)^2\}^{1/2}$ and the second term under the integral, involving the arbitrary constant a, has been added to help it converge. The equivalence (to within a constant) of Eqs. (10) and (13) may be demonstrated by expanding the first term under the integral.

4. The Free-Boundary Equilibrium Code FEQ2.5 (FR)

It is possible to use either of G_1 or G_2 in the integral expression of Eq. (9) to solve a free-boundary equilibrium. Suppose that the fixed-boundary equations have been solved inside a guessed plasma boundary, Γ_{old}, to give $\bar{\psi}_{\text{old}}$, and that $p_C = 0$ and $g_C = g_B$ on Γ_{old}. The pressure will be continuous across Γ if $\mathbf{i}_1 = 0$ as well. The contours of ψ from Eq. (9), with the integral taken over Γ_{old} and with $\mathbf{i}_1$ *set to zero* will thus give a new approximation to the actual flux surfaces. This procedure (fixed-boundary solution + Green's function integration) forms one outer loop of an iterative procedure. The algorithm has been described in detail for the toroidal case by Delucia *et al.* [11]. Our implementation for the helical case uses a version of the fixed-boundary flux coordinate code FEQ2.5 [7] which solves the equilibrium equations on a curvilinear (Ψ, Θ) grid in the top half of the $z = 0$ plane (assuming up–down symmetry). The poloidal angle (Θ) is calculated to divide each flux surface cross section (labelled by the radial coordinate Ψ) into equal arcs. The new free-boundary code, FEQ2.5 (FR), has several improvements on the toroidal case which are appropriate for "beany" heliac plasmas:

- The initial guess for the plasma shape can be taken from the contours of a vacuum magnetic field. Alternatively the code can be initialized from the results of some other converged equilibrium.

• Simple algorithms for specifying the initial flux coordinate grid, such as drawing straight lines from a local origin within the plasma to the plasma boundary, often lead to crowding in Θ for very indented surfaces. This can cause the fixed-boundary iterations to become unstable. We counter this by explicitly contouring a few of the interior flux surfaces (typically 4 out of a total of 56), rezoning them to equal arcs and using linear interpolation between them. The vacuum magnetic field is contoured using an efficient algorithm which assumes that (the cylindrical coordinate) ϕ is a single-valued function of r over each (half) surface.

• The bounding surface is defined to be a separatrix or the tangent surface to a circular limiter. The latter can be interpreted as limiting the computational region to that in which well-formed magnetic surfaces could reasonably be expected in three dimensions.

• The contouring procedure used to find the new plasma boundary involves a systematic search of the coordinate grid within region C and its extrapolation into region B. However, as an observer point approaches the old boundary, Γ_{old}, the Green's function terms in Eq. (9) develop integrable singularities. It is (tacitly) assumed by Delucia *et al.* [11] that the accuracy of their trapezoidal rule evaluation of the Green's function integral is maintained at one radial grid point either side of Γ_{old}. This will not be the case for a beany heliac plasma unless the number of Θ grid points is very much greater than the number of Ψ points. Also, because of the variation in the physical size of the radial mesh with Θ (see Fig. 2), observer points on a given flux surface will feel the effects of the singularities more acutely near the center, rather than at the tips, of the bean. Simply increasing the number of equilibrium Θ points is a very computationally expensive way of coping

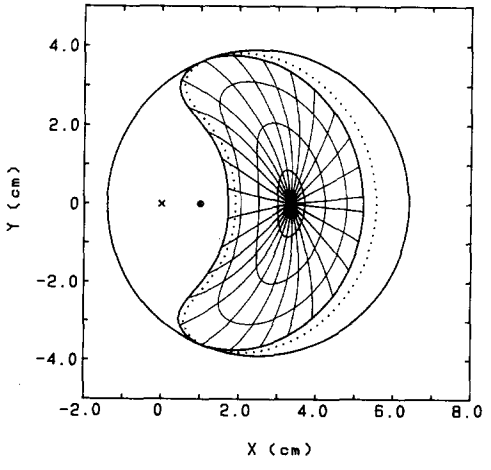

FIG. 2. Bounding surface for an $I_{xc} = 1.8$ kA, $\alpha = 2$ equilibrium at $\langle\beta\rangle = 26\%$ (dotted contour) superimposed on flux surfaces and poloidal coordinate lines for that configuration in vacuum. The circular limiter and central coil positions are also shown.

with this problem. In FEQ2.5 (FR) the Green's function integral is evaluated using the trapezoidal rule on an interpolated Θ grid (commonly increased from 56 to 276 points using cubic interpolation). As well as this, its value for observer points in a narrow region either side of, and including, Γ_{old} is estimated by cubic interpolation of its values at the edges of this region. There is, therefore, no need to integrate the singular parts of the integral explicitly.

- An efficient series representation is used for ψ_{vac}. This is discussed by Dewar and Gardner [12].

The accuracy of the free-boundary code has been estimated by computing a known vacuum field. For SHEILA equilibria (see below) with a (Ψ, Θ) grid size of 56×56 the code had a maximum error of 1% of the variation of $\bar{\psi}$ across the plasma. It is convenient to measure the convergence of the code by monitoring the position of, and value of $\bar{\psi}$ at, the magnetic axis (X_{ma} and $\bar{\psi}_{\text{ma}}$, respectively). The convergence of a $\langle\beta\rangle = 7\%$ SHEILA equilibrium to 6 decimal places in X_{ma} and 5 places in $\bar{\psi}_{\text{ma}}$ can reasonably be expected after 7 outer loops. At these sorts of pressures, with 56×56 grid points, each outer loop takes about 40 min CPU time on a FACOM-M360R or 4 min CPU time on a Cyber 205.

5. Free-Boundary SHEILA Equilibria

The SHEILA heliac has a (planar) central "core" conductor, of 18.75 cm radius, about which 24 toroidal field coils are arranged in a 3-period toroidal helix [8]. The configuration is completed by a vertical field which may be optimized to balance the shape of the flux surfaces at different toroidal angles. When this is the case the "average" shape of the flux surfaces may be approximated by a helically symmetric model, similar to Fig. 1, which has a circular solenoid of radius 6.5 cm and a helical displacement of 2.5 cm from a central line conductor [9]. Plasma is expected to be confined by a set of twisting, bean-shaped surfaces with a magnetic axis to the right of the central conductor in Fig. 1.

A recent modification to the bare SHEILA configuration is the addition of an extra helical winding on the mid-plane between the central conductor and the plasma [13]. Its current, I_{xc}, can be used as a "deformation parameter" to construct a stability diagram in the manner of Ref. [6]. As I_{xc} increases *in the opposite direction* to the main core current the plasma is pulled towards it. The flux surfaces become less indented and elongated and the total ("poloidal") rotational transform, ι, decreases (where $\iota = 1 - |\iota_h|$ and ι_h is the helical transform [7]). There is a separatrix between the helical winding and the magnetic axis.

Figure 3 is a stability diagram for a helically symmetric model of SHEILA with a core current of 16 kA in the $-z$ direction, a solenoidal field of net circulation (−)0.2048 T and a helical winding of radius 1.0 cm. The figure is a plot of flux surface shape (parametrized by I_{xc}) against $\langle\beta\rangle = 2\mu_0\langle p\rangle/B_{\text{ma}}^2$, where $\langle p\rangle$ is the average plasma pressure and B_{ma} is the magnitude of the magnetic field at the

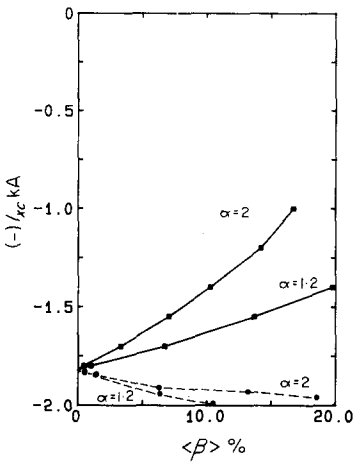

FIG. 3. Critical $\langle\beta\rangle$ for stability against ideal interchange and ballooning modes for helically symmetric, net-current-free SHEILA fixed-boundary (solid lines) and free-boundary (broken lines) equilibria. The pressure profiles have the form $p \propto \bar{\Psi}^{\alpha}$. The plasma is stable above the curves and unstable below.

magnetic axis. Note that I_{xc} increases moving down the vertical axis. The solid lines represent the critical $\langle\beta\rangle$ for stability of SHEILA equilibria when the plasma boundary is fixed to the vacuum magnetic surface which is tangential to a fictitious circular limiter of radius 3.9 cm (see Section 4). All of the equilibria had zero net longitudinal current and pressure profiles of the form $p \propto (\bar{\psi}/\bar{\psi}_{ma})^{\alpha}$. The broad $\alpha = 1.2$ pressure profiles are close to the slope of the measured profiles at very low β [8, 9], whereas $\alpha = 2$ corresponds to a peakier, bell-shaped pressure distribution [6]. The equilibrium code was run with a $56 \times 56(\Psi, \Theta)$ grid which was interpolated to a 97×128 Hamada coordinate grid for the stability analysis. The equilibria were examined for Mercier and ballooning stability using the BAL2.5 code [7]. None of the equilibria in this parameter space is in the "second stability region" to interchange modes [6] so that the stability boundaries against ideal Mercier and ideal ballooning modes coincide.

As the pressure is increased, the magnetic axis shifts away from the central conductors and the elongation (and total rotational transform) of the innermost flux surfaces increases. (At an $\langle\beta\rangle$ of 24% the magnetic axis of an $I_{xc} = 2$ kA, $\alpha = 2$ equilibrium had shifted 19% of the distance from the vacuum magnetic axis to the boundary). For some values of I_{xc} in the fixed boundary case there is a transition to a Mercier unstable configuration with increasing β. Above the marginal point at zero pressure the magnitude of the specific volume, V', decreases monotonically from the magnetic axis to the separatrix. Thus V'' is negative everywhere which is equivalent to there being a continuous magnetic well across the plasma [14]. The marginal point coincides with the appearance (with increasing I_{xc}) of a magnetic hill close to, but not exactly at, the magnetic axis in an equilibrium which otherwise

has a net magnetic well. As I_{xc} is increased the hill moves into the magnetic axis but there is still a net magnetic well. Close to the marginal point, the transition to Mercier instability with increasing β first takes place close to, but not exactly at, the magnetic axis. The stability boundary has a greater dependence on pressure profile than that noted by Ref. [6].

The critical $\langle\beta\rangle$ for free-boundary SHEILA equilibria are shown as the broken lines in Fig. 3. The free-boundary runs were initialized with a vacuum grid and run for between 4 and 7 outer loops. As the pressure is increased, with the coil currents and limiter position held fixed, the plasma shifts outwards and broadens (Figs. 2 and 4). We have found that the increase in the helical aspect ratio, though small to the eye, is sufficient to stabilize all those fixed-boundary SHEILA configurations for which there is a transition to instability at finite pressure. In other words, any zero-pressure configuration with a magnetic well everywhere will remain stable as the $\langle\beta\rangle$ is increased. Note that, as with the fixed boundary case, the shallower pressure profile is more stable and the most Mercier-unstable region of the plasma is close to the magnetic axis. The stabilizing effect of increasing the helical aspect ratio has been predicted by Ref. [6].

We have compared our prediction of the shape of the V' profile near the marginal point at zero pressure with the results of a 3D field line tracing code. It has been shown that there are configurations near the marginal point of the (fully toroidal) SHEILA heliac for which the V' profile changes from a hill at the magnetic axis to a well across some of the intermediate flux surfaces and back to a hill at the edge. In the helically symmetric case there must always be an overall magnetic well because the closest bounding separatrix (introduced by the extra helical winding) has an x point (of radius r_x) between the z-axis and the magnetic

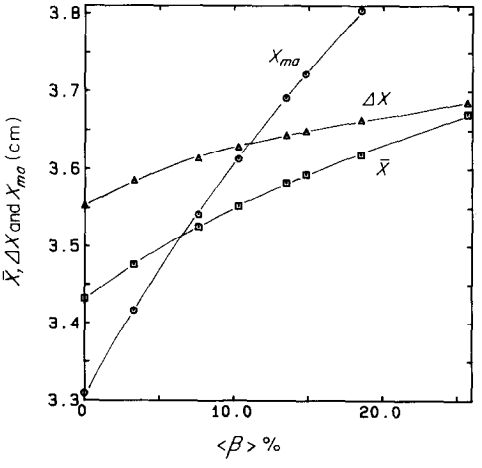

FIG. 4. Midpoint ($\bar{X}$), width (ΔX) and magnetic axis position (X_{ma}) as a function of $\langle\beta\rangle$ for $I_{xc} = 2$ kA, $\alpha = 2$ free-boundary equilibria.

axis (radius r_{ma}). (The ratio of the specific volumes, V', of the magnetic axis and this separatrix can be shown to be [14]

$$Q = \frac{1 + h^2 r_{ma}^2}{1 + h^2 r_x^2}$$

and Q will always be greater than one in this case.) In the toroidal case there will often be a magnetic hill near the outside of a set of nested flux surfaces even if there is a well at the magnetic axis. This effect is probably due to the influence of the magnetic field ripple introduced by a discrete set of toroidal field coils [15] but is sometimes obscured by surface breakup.

There are several intrinsically 3D characteristics of closed toroidal stellators (notably the coupling of toroidal and helical curvatures, the change in flux surface shape with the toroidal angle, the effects of coil discretization, and the possible existence of magnetic islands near rational values of the rotational transform) which cannot be modelled in this helically symmetric treatment. Although a detailed discussion of these effects is outside the scope of this paper it should be noted that the principal result of Fig. 3, that the outwards shift of the SHEILA plasma will stabilize Mercier and ballooning modes, will depend on to what extent a helical shift is dominant over a toroidal shift. Because the magnitudes of the toroidal and helical shifts are inversely proportional to the square of their respective (poloidal or helical) rotational transforms (as well as being directly proportional to their respective aspect ratios) [6, 16], one would expect that the helically symmetric model would be most accurate when $\iota \gg \iota_h$. To approach this regime in the present case one could run the current in the extra helical winding in the same direction as the core current which would put the configuration in the quiescently stable region of Fig. 3. There are indications from some 3D studies that a "helical" optimization of the toroidal heliac may be preferable for MHD equilibrium and stability as well as transport [17].

ACKNOWLEDGMENTS

The authors acknowledge the support of the CSIRO Computing Grants Scheme. We wish to thank Dr. D. A. Monticello for making the FEQ2.5 code available to us and Dr. B. D. Blackwell and Ms. X. H. Shi for running the field-line tracing code. We also wish to acknowledge useful discussions with Drs. B. D. Blackwell, B. A. Carreras, and S. M. Hamberger. H. J. Gardner gratefully acknowledges the support of a Commonwealth Postgraduate Research Award and an A.N.U. Supplementary Scholarship.

REFERENCES

1. S. P. HIRSHMAN, W. I. VAN RIJ, AND P. MERKEL, *Comput. Phys. Commun.* **43**, 143 (1986).
2. F. BAUER, O. BETANCOURT, AND P. GARABEDIAN, *Magnetohydrodynamic Equilibrium and Stability of Stellarators* (Springer–Verlag, New York, 1984).

3. A. E. KONIGES AND J. L. JOHNSON, *Phys. Fluids* **28**, 3127 (1985).
4. R. GRUBER, W. KERNER, P. MERKEL, J. NÜHRENBERG, W. SCHNEIDER, AND F. TROYON, *Comput. Phys. Commun.* **24**, 389 (1981).
5. P. MERKEL, J. NÜHRENBERG, R. GRUBER, AND F. TROYON, *Nucl. Fusion* **23**, 1061 (1983).
6. D. A. MONTICELLO, R. L. DEWAR, H. P. FURTH, AND A. REIMAN, *Phys. Fluids* **27**, 1248 (1984).
7. R. L. DEWAR, D. A. MONTICELLO, AND W. N-C. SY, *Phys. Fluids* **27**, 1723 (1984).
8. B. D. BLACKWELL, S. M. HAMBERGER, L. E. SHARP, AND X. H. SHI, *Nucl. Fusion* **25**, 1485 (1985).
9. H. J. GARDNER, Ph.D. thesis, Australian National University, 1986 (unpublished).
10. J. D. JACKSON, *Classical Electrodynamics* (Wiley and Sons, New York, 1982).
11. J. DELUCIA, S. C. JARDIN, AND A. M. TODD, *J. Comput. Phys.* **37**, 183 (1980).
12. R. L. DEWAR AND H. J. GARDNER, The Eigenfunction Expansion for the Helical Solenoid, Report ANU/TPP86/03 (unpublished); *J. Comput. Phys.*, in press.
13. J. H. HARRIS, J. L. CANTRELL, T. C. HENDER, B. A. CARRERAS, AND R. N. MORRIS, *Nucl. Fusion* **25**, 623 (1985).
14. B. MCNAMARA, K. J. WHITEMAN, AND J. B. TAYLOR, *Plasma Physics and Controlled Nuclear Fusion Research*, Vol. 1, p. 103 (IAEA, Vienna, 1966).
15. B. D. BLACKWELL, private communication.
16. S. YOSHIKAWA, Princeton Plasma Physics Laboratory Report No. PPPL–1829, 1981 (unpublished).
17. B. A. CARRERAS, private communication.